Transport and magnetic properties of La 0.7 Pb 0.3 MnO 3 +x Ag (x=0−20 wt %) nanocomposites

Sudipta Pal, Aritra Banerjee, S. Chatterjee, A. K. Nigam, B. K. Chaudhuri, and H. D. Yang

Citation: Journal of Applied Physics **94**, 3485 (2003); doi: 10.1063/1.1597761
View online: http://dx.doi.org/10.1063/1.1597761
View Table of Contents: http://scitation.aip.org/content/aip/journal/jap/94/5?ver=pdfcov
Published by the AIP Publishing

Transport and magnetic properties of $La_{0.7}Pb_{0.3}MnO_3+x$ Ag ($x=0-20$ wt%) nanocomposites

Sudipta Pal and Aritra Banerjee[a)]
Department of Solid State Physics, Indian Association for the Cultivation of Science, Jadavpur, Kolkata-700 032, India

S. Chatterjee and A. K. Nigam
Department of CMP and MS, Tata Institute of Fundamental Research, Mumbai-400 004, India

B. K. Chaudhuri[b)]
Department of Solid State Physics, Indian Association for the Cultivation of Science, Jadavpur, Kolkata-700 032, India

H. D. Yang
Department of Physics, National Sun Yat Sen University, Kaohsiung-804, Taiwan, Republic of China

(Received 31 October 2002; accepted 10 June 2003)

Magnetization and transport properties of $La_{0.7}Pb_{0.3}MnO_3+x$ Ag ($x=0-20$ wt%) nanocomposites have been reported. In this Ag-containing colossal magnetoresistive (CMR) $La_{0.7}Pb_{0.3}MnO_3$ composite (referred to as CMR-Ag), conductivity (σ) and metal–insulator transition temperature (T_p) increase with increasing Ag. Electron microscopy and elemental mapping indicated a uniform distribution of Ag nanoparticles/clusters. The enhancement of T_p is accompanied by a reduction of the *c*-axis lattice constant. Coexistence of interfacial tunneling with intrinsic transport behavior has been observed at the grain boundaries in the samples with a higher ($\geqslant$10 wt%) Ag content. Due to the presence of nonmagnetic Ag in the ferromagnetic $La_{0.7}Pb_{0.3}MnO_3$ material, dc magnetization decreases but the corresponding T_p increases. In the low-temperature ($T<T_p$) phase, resistivity data follow a T^2 dependent behavior for the samples with higher Ag concentration ($x\leqslant 5$ wt%). On the other hand, for lower Ag ($\leqslant$5 wt%) containing samples, a $T^{2.5}$ dependent behavior is observed. This suggests the importance of both the electron–electron (T^2 dependence behavior) and the electron–magnon ($T^{2.5}$ dependence behavior) interactions for explaining low-temperature ($T<T_p$) transport data of the CMR-Ag nanocomposites. In the insulating (semiconducting) regime ($T>T_p$), conductivity data follow the adiabatic polaron hopping conduction mechanism. Unlike the Ag free sample, the variable-range-hopping model is found to be inapplicable for the present Ag containing nanocomposites. © *2003 American Institute of Physics.* [DOI: 10.1063/1.1597761]

I. INTRODUCTION

The colossal magnetoresistive (CMR) manganites of the type $Re_{1-x}A_xMnO_3$ (Re= rare earth, A=Ca, Sr, Ba, or Pb) with a perovskite structure have drawn considerable interest in recent years.[1–5] This is because of their striking electrical and magnetic properties as well as their technological importance. Various attempts are being made to understand the effect of nonmagnetic ion doping on the transport and magnetic properties in these manganites. It has been observed[6,7] that the addition of nonmagnetic Ag in the polycrystalline films of a CMR material improves the microstructure of the surface, oxygen concentration, electrical, and magnetic homogeneities. The presence of Ag also reduces conduction noise. Earlier investigations indicated[8,9] that Ag is one of the most suitable doping elements for improving superconducting properties of the bulk high T_C cuprate superconductor [like $YBa_2Cu_3O_7$(YBCO)]. As the lattices of the YBCO-type superconductor did not accommodate Ag atoms, it was then concluded that Ag atoms segregated at the intergranular region moving out of the growing grains.[10] This ultimately enhances the grain-boundary conductivity with the improvement of oxygen concentration as well as the uniformity of the grain size in YBCO superconductor. Similar types of effects are also expected in the bulk CMR materials of our present investigation. It has also been reported recently[11–13] that the introduction of a nonmagnetic or an antiferromagnetic impure phase into the ferromagnetic manganite matrix leads to an increase of the room-temperature magnetoresistance. This observation has also encouraged us to study the effect of nonmagnetic Ag addition into the ferromagnetic manganite matrix. It is noticed that preparation of uniform nanosize grains ($\sim$20 nm or less) of the CMR material is possible with the addition of Ag. Since the addition of Ag highly influences the oxygen concentration in the lattice, grain size, nature of the grain boundary, the study of resistivity, and magnetization of the bulk CMR-Ag composite sample is, therefore, interesting.

a)Present address: Physical Metallurgy Section, Indira Gandhi Center for Atomic Research, Kalpakkam-603102, Tamilnadu, India.
b)Author to whom correspondence should be addressed; also at Department of Physics, National Sun Yat Sen University, Kaohsiung-804, Taiwan, ROC; electronic mail: sspbkc@mahendra.iacs.res.in

For the study of a CMR-Ag nanocomposite, we have selected the well studied La–Pb–Mn–O-type CMR material showing[1,4,5,14] metal–insulator transition (MIT) near room temperature. We have prepared $La_{0.7}Pb_{0.3}MnO_3$ with the addition of different concentrations of Ag (0–20 wt %). Structure, temperature dependent transport, and magnetic properties of all of these Ag (0–20 wt %) added composites have been studied. These composite samples show a small increase of grain size (from ~17 to 20 nm) with a large increase of the corresponding MIT temperature T_p. The behavior of the higher ($\geqslant$10 wt %) Ag-containing samples is found to differ appreciably from that of the lower Ag-containing samples. For a better understanding of the transport mechanism in this ferromagnetic–nonmagnetic nanocomposite system, both in the low ($T<T_p$) and high ($T>T_p$) temperature regions, conductivity data have been consistently analyzed using the appropriate theoretical models.

II. EXPERIMENT

A series of bulk polycrystalline $La_{0.7}Pb_{0.3}MnO_3+x$ Ag ($x=0-20$ wt %) samples were prepared by conventional solid-state reaction method similarly to our earlier work.[5] High-purity (99.99%) La_2O_3, PbO, $Mn(CH_3COO)_3$, and $AgNO_3$ powders were mixed well in appropriate stoichiometric ratio and ground. The well-mixed powders were preheated at a temperature of 773 K for 6 h. Then, it was successively heated at 1073 K for 24 h and at 1173 K for 24 h with intermediate grindings. The pelletized samples were finally sintered at 1073 K for 12 h and then slowly furnace cooled to room temperature. All of the samples of different compositions were characterized by x-ray diffraction (XRD) studies with Cu $K\alpha$ ($\lambda=1.541$ Å) radiation. Temperature dependent resistivity and magnetoresistance of the samples were measured by standard four-probe technique in the temperature range of 80–400 K (maximum magnetic field used 1.5 T) similar to our earlier work.[5] Temperature was measured with an accuracy ± 0.5 K. The low-temperature magnetization of the sample (down to 4 K) was measured by a Vibrating Sample Magnetometer (Oxford instruments).

III. RESULTS AND DISCUSSION

The XRD patterns of the Ag-containing composite samples are shown in Fig 1. It is found from Fig. 1 that for higher values of Ag concentrations (5 wt %), some extra peaks of Ag appear along with the perovskite peaks. A microstructure similar to a $La_{1-x}Ag_xMnO_3$ film was also reported by Tao *et al.*[15] The composite system of our present investigation is, however, different from the sample studied by Tao *et al.*[15] From the XRD patterns shown in Fig. 1, it also appears that Ag is present in the intergranular region[6] in the form of nanoparticles/clusters. This is also visualized from the elemental mapping of a small region of the sample as shown in Fig. 2 for a typical sample with $x=10$ wt % Ag. Figure 2 also shows the uniform distribution of Ag particle/cluster in the sample. In its perovskite phase, the average grain size of the sample was estimated from the XRD data. For this purpose, we used the modified Scherrer relation viz. $S=K\lambda/\beta\cos\theta$, where $\lambda=1.541$ Å is the wavelength of the

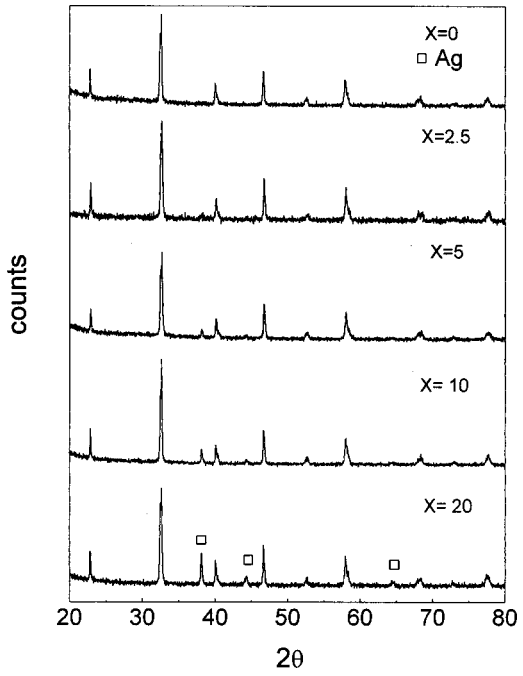

FIG. 1. XRD patterns of $La_{0.7}Pb_{0.3}MnO_3+x$ wt % Ag with $x=0$, 10, and 20 wt %, respectively. The peaks due to Ag are marked with □.

Cu $K\alpha$ radiation, β is the full width at half maximum (FWHM) of the XRD peak, and K is a constant depending on grain shape ($=0.89$, assuming circular grain). The estimated average grain size of the samples varied from 17–20 nm (depending on Ag concentrations) as shown in Table I. The average grain sizes of the Ag particle/clusters in different samples with Ag$>$5 wt % have also been estimated from the FWHM of the XRD peak of Ag. For all of these samples, the average size of the Ag grains is found to be about 20 nm, almost equal to the size of the CMR particles.

Figure 3 shows the thermal variation of magnetization at 5 kOe for the $La_{0.7}Pb_{0.3}MnO_3+x$ Ag ($x=0$, 10, and 20 wt%) composite samples. It is seen that magnetization decreases with increasing Ag content. However, the Curie temperature T_C of the sample increases with an increase in Ag content (viz. $T_C\sim317$ K, ~341 K, and ~361 K, respectively, for $x=0$, 10, and 20 wt % observed from the high-temperature magnetic measurement). The observed increase of T_C with the addition of Ag agrees well with other reported results.[8,9]

Figure 4 represents temperature dependent resistivity of the composites for different concentrations of Ag. Resistivity peak (at T_p) of the Ag-free sample (viz. $La_{0.7}Pb_{0.3}MnO_3$) is observed at 235 K, which is lower than that of the previously reported value (~320 K). [16,17] This is due to smaller grain size (~17 nm) of the sample of our present investigation. When the grain size is small enough, spin dependent tunneling may dominate in the transport mechanism. So the resistivity peak of the Ag-free $La_{0.7}Pb_{0.3}MnO_3$ sample occurs far below the corresponding Curie temperature.[18] Resistivity of the sample decreases with the addition of silver and the corresponding T_p shifts to a higher-temperature region.

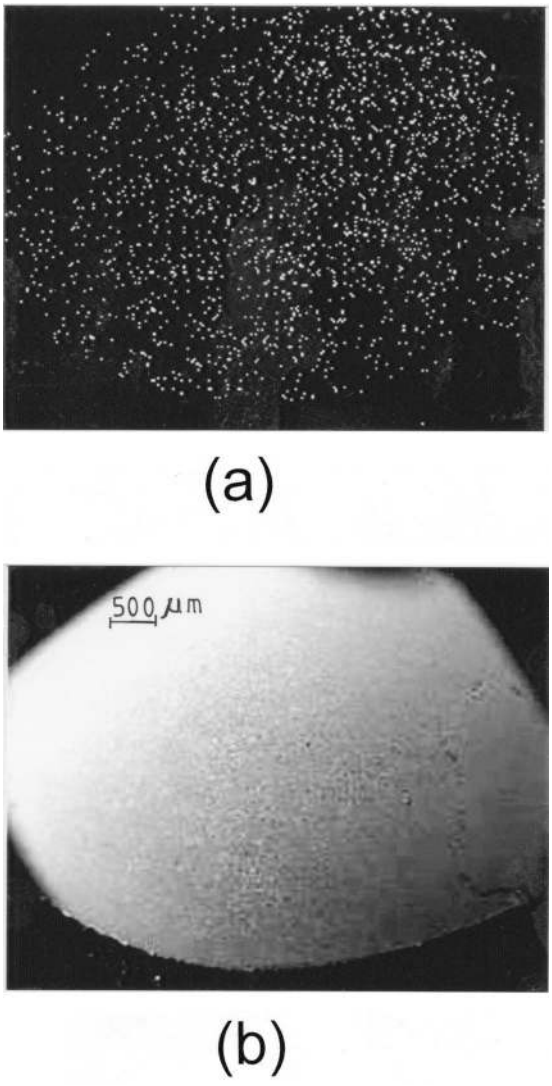

FIG. 2. Elemental mapping of Ag in a typical sample $La_{0.7}Pb_{0.3}MnO_3$ + 10 wt % Ag showing uniform distribution of Ag cluster in sample (a). Scanning electron microscopy image of the sample in the same scale is given for reference (b).

It is well known[5] that the conductivity of the polycrystalline granular system increases with the corresponding increase of the grain size. But, in the present composite samples, the grain size does not vary appreciably with the addition of Ag. So, it is reasonable to assume that oxygen content of the grain might also be one of the key factors that would lead to the observed increase in conductivity. Previous

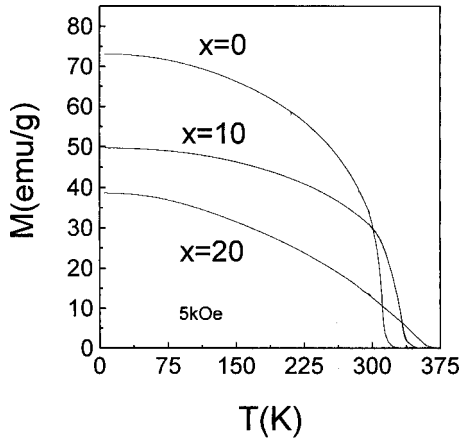

FIG. 3. Thermal variation of dc magnetization of ($La_{0.7}Pb_{0.3}MnO_3$ + x wt % Ag) with $x = 0$, 10, and 20 wt %, respectively, in magnetic field (B) 5 kOe.

studies on Ag-doped La–Ca–Mn–O films[6] and on bulk materials established the correlation between the oxygen content in the films and the higher values of T_p. It was also shown[6] that the increase of oxygen content resulted in a decrease of c-axis lattice parameter. We have also examined the structural change to infer the variation of the oxygen content of the present system. The crystal structure of Ag-free $La_{0.7}Pb_{0.3}MnO_3$ sample is found to be rhombohedral (space group $R\bar{3}C$ with a hexagonal unit cell) with lattice constants $a = 5.5167$ Å and $c = 13.4048$ Å. These values of lattice constants agree fairly well with those reported[14] earlier for a similar sample. In Fig. 5, the c-axis lattice parameters of the samples are shown as a function of T_p. It is seen from Fig. 5 that the enhancement of T_p is accompanied by a reduction of the c-axis lattice constant.

The behavior of the temperature dependent resistivity curve of the low Ag (< 10 wt %)-containing nanocomposite samples are quite different from that of the corresponding higher Ag ($x = 10$ and 20 wt %)-containing samples. For the samples with higher Ag concentrations, the resistivity peak is observed at a much higher temperature (~335 K for $x = 10$ and 20 wt %). A shoulderlike nature of the resistivity curve appears around the temperature T^* (say) which lies a little below T_p as shown in Fig. 4 for the sample with $x = 10$ wt %. This behavior of the present nanocomposite samples, with higher Ag content, can be explained by considering the coexistence of interfacial tunneling and spin-related intrinsic transport at the grain boundaries similar to

TABLE I. Grain size dependent transport parameters obtained from fitting the conductivity data of $La_{0.7}Pb_{0.3}MnO_3$ + x wt % Ag ($x = 0$, 2.5, 5, 10, and 20) with Eq. (1).

x (wt %) Ag	Grain size[a] S (in nm)	$\theta_D(K)$	ν_0(Hz)	E_p (meV)	$\sigma_0(S\ cm^{-1})$ (at 300 K)
0.0	17.7	590	1.22×10^{13}	158.5	1.37×10^{2}
1.25	18.0	600	1.25×10^{13}	134.0	1.78×10^{2}
2.5	18.3	610	1.27×10^{13}	122.6	1.82×10^{2}
5.0	20.6	646	1.34×10^{13}	124.2	6.49×10^{2}
10.0	20.8	660	1.37×10^{13}	94.7	8.95×10^{2}
20.0	19.3	660	1.37×10^{13}	96.6	9.02×10^{2}

[a]Average grain size measured from XRD

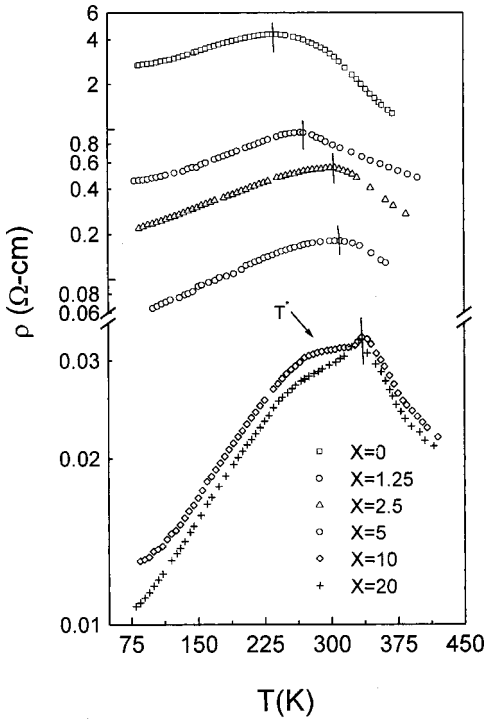

FIG. 4. Thermal variation of resistivity (ρ) of $La_{0.7}Pb_{0.3}MnO_3+x$ wt % Ag ($x=0-20$ wt %) showing MITs for all of the samples. Transition temperature is marked with a straight line. A typical nature of the curve just below T_p (indicated by T^*) for the sample with higher Ag concentration, viz. 10 wt % and 20 wt % Ag indicates the existence of interfacial tunneling of conducting electron.

that reported in the earlier papers.[18–20] Previously, the shoulderlike nature had been observed[18–20] for a particular grain size. In our present system, this nature is, however, observed for samples with a particular Ag concentration ($x=10$ wt %). The temperature dependent resistivity curve also indicates that with the decrease of scattering by the defects, as well as by the grain boundaries, the role of the spin-related intrinsic transport becomes more prominent. If Ag concentration is around 20 wt %, conductivity is less than that of the previous one ($x=10$ wt %, say) and the resistivity peak becomes sharper, which reflects the dominant effect of

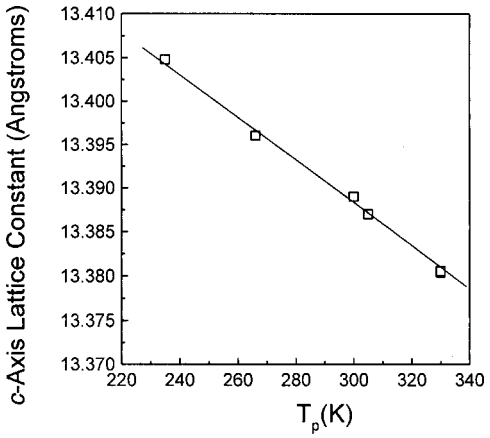

FIG. 5. Linear variation of c-axis lattice constant with enhancement of T_p in $La_{0.7}Pb_{0.3}MnO_3+x$ wt % Ag with $x=0-20$ showing a reduction of c-axis lattice constant with an increase of silver concentration.

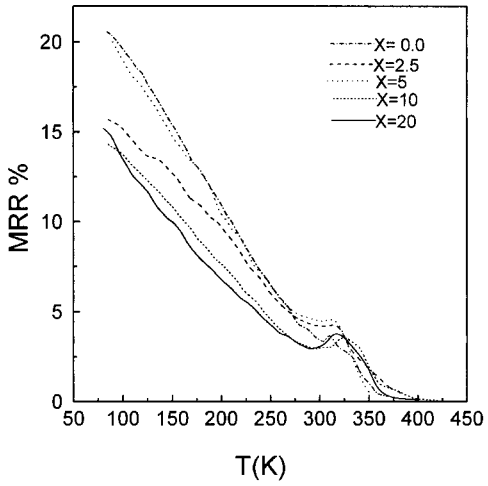

FIG. 6. MRR ($MRR=-(\rho_{1.5}-\rho_0)/\rho_0$) as a function of temperature for the samples $La_{0.7}Pb_{0.3}MnO_3+x$ wt % Ag with $x=0$, 2.5, 10, and 20. All of the samples show a peak around 320 K which arises due to magnetic ordering between Mn^{3+} and Mn^{4+}.

intrinsic double-exchange interaction. However, an elaborate investigation is needed to focus more light on this typical behavior of the nanocomposites.

The magnetoresistance ratio MRR $[=-(\rho_{1.5T}-\rho_{0T})/\rho_{0T}]$ of the present nanocomposite sample shown in Fig. 6 indicates that the low-temperature (~ 80 K) MRR decreases with increasing Ag concentration. Except for the samples with $x=2.5$ and 5 wt % Ag, the room-temperature (~ 300 K) MRR values are little lower than that of the corresponding Ag-free sample. It is worthwhile to mention here, that for the aforementioned two samples (i.e., $x=2.5$ and 5 wt %), MIT also occurred near room temperature (Fig. 4). A small peak in the MRR (Fig. 6) curve around T_c is noticed for all of the samples. Interestingly, the corresponding peak temperatures of MRR curves do not show a significant change with the increase of Ag concentration (or grain size). The peak in the MRR curve arises due to the change in magnetic ordering (paramagnetic to ferromagnetic with the lowering of temperature) between Mn^{3+} and Mn^{4+} ions. This also indicates that the ratio Mn^{3+}/Mn^{4+} does not change with increase of Ag concentration in the samples.[5]

The conductivity data (Fig. 7) in the high-temperature ($T>T_p$) phase are well fitted with the small-polaron-hopping (SPH) conduction mechanism.[21] According to this model, the expression for conductivity is given by

$$\sigma(T)=\frac{\sigma_0}{T^n}\exp(-E_p/k_BT)=\frac{g_d e^2 \nu_0}{a k_B T^n}\exp(-E_p/k_BT), \tag{1}$$

where a and E_p are, respectively, the jump distance and the activation energy of the polaron, ν_0 is the characteristic phonon frequency, and g_d is a constant that depends on the lattice structure. $n=1$ indicates adiabatic hopping of polaron while for nonadiabatic hopping, $n=3/2$. To elucidate the nature of charge transport mechanism above the MIT temperature regime, $\ln(\sigma T)$ has been plotted as a function of 1000/T (Fig. 7). This plot shows Arrhenius behavior of the conductivity (σ) in the semiconducting phase ($T>T_p$). An indica-

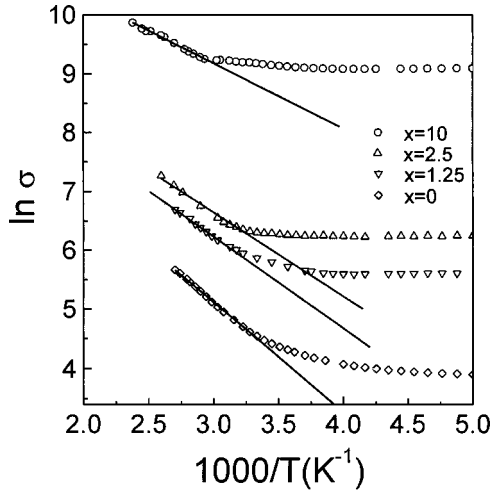

FIG. 7. Variation of $\ln\sigma T$ as a function of inverse temperature 1000/T for $La_{0.7}Pb_{0.3}MnO_3 + x$ wt % Ag ($x = 0$, 1.25, 2.5, 5, 10, and 20) above the respective, MIT, temperatures. Solid lines indicate the best fit of the experimental data with Eq. (1).

tion about the nature of hopping (adiabatic or nonadiabatic) is obtained from the value of σ_0 [Eq. (1)]. For adiabatic hopping, the prefactor (σ_0) approaches a typical value of $6.99\times10^2\ \mathrm{Scm}^{-1}$ at $kT = h\nu_0$ and for nonadiabatic σ_0 is much smaller than the aforementioned critical value.[22] The estimated values of $\sigma_0(\sim10^2)$ for all the composite samples of our present investigation given in Table I indicate that σ_0 lies close to the theoretical limit given herein, which suggests adiabatic polaron-hopping conduction mechanism for all of the samples.

At a particular temperature, where the curve (in Fig. 7) shifts from its straight-line behavior, is usually noted as $\theta_D/2$ (where θ_D is the Debye temperature). The estimated values of θ_D for the samples are shown in Table I. The characteristic phonon frequency ν_0 estimated from the relation $k\theta_D = h\nu_0$ is also shown in Table I for comparison. It was shown earlier[4,5] that the region between T_p and $\theta_D/2$ could be explained with variable-range-hopping (VRH) model for the Ag-free $La_{0.7}Pb_{0.3}MnO_3$. For the Ag containing samples, however, this region is found to be very small and VRH model cannot be applied. It is seen from Table I that the values of $\theta_D/2$ shift toward T_p (as resistivity decreases and T_p increases with increase of Ag concentration). The SPH model [Eq. (1)] is found to fit the experimental conductivity data well for the entire high-temperature (above T_p) range (semiconducting region). It is significant to note that for the Ag-containing nanocomposite sample where the MIT temperature is quite high ($\sim$335 K), the VRH model becomes almost inapplicable. The SPH model is found be sufficient and the most suitable one for explaining the conductivity data above the MIT temperature. With the increase of Ag content in the samples, activation energy E_p [estimated from Eq. (1)] decreases (Table I) and attains a minimum value for the sample with $x = 10$ wt % Ag. Improvement of intergranular connectivity by Ag addition caused the activation energy to decrease. Here, we must mention that the activation energy also decreases (increasing conductivity) with the application of magnetic field, which can be interpreted on the basis of the alignment of magnetic spins and, hence, the increase of conductivity.

On the other hand, conductivity data of all the samples in the low-temperature ferromagnetic regime ($T < T_p$) show metallic behavior (Fig. 4), and the data have been fitted with different theoretical expressions[19,23–26] to find the best-fitted one. From such a fitting, signatures of different types of interaction terms (viz., electron–electron, electron–magnon, or electron–phonon) are found to govern the transport mechanism in the low-temperature phase ($T < T_p$). Temperature dependent resistivity data in this region, where the local ferromagnetic order is almost complete, have been fitted with

$$\rho = \rho_\alpha + \rho_m T^m, \tag{2}$$

where the temperature independent part ρ_α is the resistivity due to domain, grain-boundary, and other temperature independent scattering mechanisms. The term $\rho_{2.5}T^{2.5}$ [for $m = 2.5$ in Eq. (2)] arises from the electron–magnon scattering process.[19] When $m = 2$ [Eq. (2)], the term $\rho_2 T^2$ corresponds to an electron–electron scattering[23] process. We have attempted to fit the low-temperature data ($T < T_p$) with both the expressions obtained for $m = 2.5$ and 2.0. Interestingly, it is observed that the conductivity data of all of the samples with different Ag concentrations could not be fitted with a single expression of the form $\rho = \rho_\alpha + \rho_2 T^2$ or $\rho = \rho_\alpha + \rho_{2.5}T^{2.5}$ (see Fig. 8). A critical analysis of the low-temperature conductivity data indicates that for the highly Ag-doped samples (i.e., $x \geqslant 5$ wt % Ag), equation $\rho = \rho_\alpha + \rho_2 T^2$ fits the conductivity data well indicating the importance of electron–electron scattering. On the other hand, for lower Ag-doped samples ($x = 0$, 1.25, and 2.5 wt %), the corresponding resistivity data are well fitted with the equation $\rho = \rho_\alpha + \rho_{2.5}T^{2.5}$, which indicates the importance of the electron–magnon scattering in the same low-temperature metallic phase. It was reported earlier[4,19] that the samples with larger values of $\rho_\alpha(\sim1$ ohm cm) followed the $T^{2.5}$ dependent behavior, whereas the systems with much lower $\rho_\alpha(\sim10^{-3}$ ohm cm), followed a T^2 dependence.[27] For the sample with $x \geqslant 5$ wt % Ag, the estimated values of ρ_2 (given in Table II) are comparable with those obtained earlier for the $La_{1-x}Sr_xMnO_3$ ($x = 0.2-0.4$) system.[27] But for the Ag-free sample, the values of $\rho_{2.5}(\sim10^{-6})$ are comparable with those obtained for the $La_{0.5}Pb_{0.5}Mn_{1-x}Cr_xO_3(x = 0.0-0.5)$[4] and $La_{2/3}Ca_{1/3}MnO_3$ (Ref. 26) systems both having $\rho_\alpha \sim 1$ ohm cm. So, it can be said that in the low-temperature metallic phase ($T < T_P$), the scattering process changes from electron–magnon to electron–electron with the decrease of resistivity (due to the increase of Ag concentration). Here, we should also mention that electron–phonon interaction seemed to be not very important in the low-temperature regime. Typically, in metal, the strength of the electron–phonon interaction is such that $\Delta\rho\,(\sim300\ \mathrm{K})[=\rho_{300\mathrm{K}} - \rho_{4.2\mathrm{K}}] \leqslant 100\ \mu\Omega$ cm. In metallic oxides, $\Delta\rho\,(\sim300\ \mathrm{K})$ is generally $\leqslant 1-3\ m\Omega$ cm. In the manganites, in the metallic region ($T < T_p$), $\Delta\rho\,(T_C)[=\rho_{300\mathrm{K}} - \rho_{4.2\mathrm{K}}]$ is much larger. For example, in $La_{1-x}Ca_xMnO_3$ and $LaMnO_3$, the observed values of $\Delta\rho$ are ~3 and $4\,\Omega$ cm, respectively. In the present Ag-containing $La_{0.7}Pb_{0.3}MnO_3$ system, this value of $\Delta\rho$ is found to be greater than 20–30 $m\Omega$ cm (depending on Ag

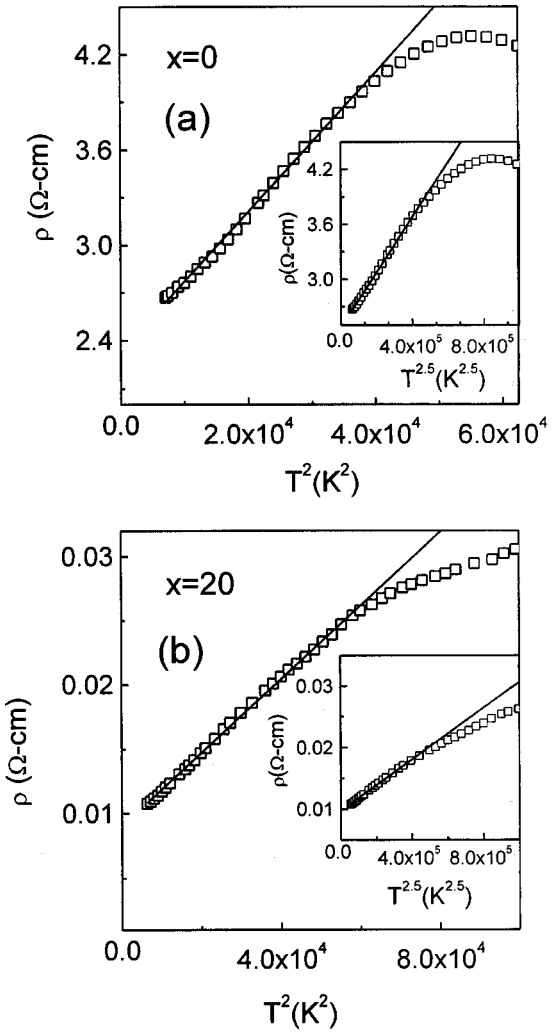

FIG. 8. Low-temperature resistivity data of two typical samples $La_{0.7}Pb_{0.3}MnO_3 + x$ wt % Ag (for $x = 0$ and 20) fitted with the expression $\rho_\alpha + \rho_2 T^2$ and $\rho_\alpha + \rho_{2.5} T^{2.5}$ [Eq. (2)]. Solid lines indicate the best fit of the experimental data. The fitting lines show the first expression fits better for the samples with $x = 20$ wt %.

concentration), which is very large with respect to that of a typical metal. So one can disregard the importance of electron–phonon interaction for the explanation of temperature dependence of ρ in the low-temperature region: The best-fit parameters obtained from fitting the low-temperature conductivity data with Eq. (2) (for $m = 2$) are shown in Table II. One finds from Table II that ρ_α decreases significantly with magnetic field. As the magnetic field increases, the size of the domain boundary decreases, and ρ_α becomes smaller. The observed very small magnetic field dependence of ρ_2 in the second term of Eq. (2), which signifies electron–electron scattering process,[28] however, needs further explanation.

IV. SUMMARY AND CONCLUSION

In summary, we have studied the effect of Ag addition in the $La_{0.7}Pb_{0.3}MnO_3$ polycrystalline samples with nanometer grain/cluster sizes ($\sim 17-20$ nm). These samples are termed as CMR-Ag nanocomposites. Both resistivity and magnetization decrease with the addition of Ag, particularly for the samples with lower Ag concentrations (Ag < 10 wt %). The ferromagnetic Curie temperature of the sample increases with an increase of Ag concentration. The presence of Ag in the form of nanoclusters at the intergranular position improves the connectivity between different grains. The MIT temperature (T_p), as well as grain size, increases with Ag addition. Moreover, intergrain conductivity and oxygen concentration of the samples also improved due to Ag addition and, as a consequence, conductivity of the nanocomposite increases. Above the MIT temperature, resistivity data follow adiabatic SPH conduction for all the samples. Unlike many other CMR materials, the VRH model is found to be not applicable in this region ($T > T_p$) for the CMR-Ag composites. In the low-temperature regime (below T_p), the T^2 dependence of the resistivity data is more prominent than the corresponding $T^{2.5}$ dependence behavior, particularly for the samples with higher Ag ($x > 5$ wt %) contents. This indicates that the electron–electron scattering (T^2 dependence) dominates with the increase of Ag contents and, hence, with the decrease of resistivity. The thermal variation of resistivity data also shows that interfacial spin dependent-type tunneling appears for higher Ag-containing samples. A more elaborate study of this type of CMR nanocomposite would be interesting. Moreover, varying Ag concentration, both T_p and T_C of the CMR-Ag nanocomposite samples could be varied over a wide range of temperature. This property might be important for technological application.

TABLE II. The values of the parameters obtained from fitting the low-temperature ($T < T_P$) conductivity data with Eq. (2) (taking $m = 2$) both in presence and in absence of magnetic field.

	ρ_α(Ω cm)		ρ_2(Ω cm K^2)	
x wt % Ag	0.0 T	1.5 T	0.0 T	1.5 T
0.0	2.343	1.766	40×10^{-6}	50×10^{-6}
1.25	0.384	0.297	8.5×10^{-6}	8.41×10^{-6}
2.50	0.184	0.149	5.1×10^{-6}	5.61×10^{-6}
5.00	0.066	0.049	1.87×10^{-6}	1.9×10^{-6}
10.00	0.010	0.008	2.93×10^{-7}	3.03×10^{-7}
20.00	0.009	0.007	2.85×10^{-7}	2.93×10^{-7}

ACKNOWLEDGMENTS

The authors acknowledge the Department of Science and Technology, Govt. of India for financial support to perform this work. One of the authors (B. K. C.) also gratefully acknowledges the partial financial help from NSC, Taiwan, during his visit at the National Sun Yat Sen University.

[1] R. Mahendiran, R. Mahesh, A. K. Roychaudhuri, and C. N. R. Rao, J. Phys. D **28**, 1743 (1995).
[2] J. M. D. Coey, M. Viret, and S. von Molnar, Adv. Phys. **48**, 167 (1999).
[3] R. Mahendiran, S. K. Tiwary, A. K. Roychaudhuri, T. V. Ramakrishnan, R. Mahesh, N. Rangavittal, and C. N. R. Rao, Phys. Rev. B **53**, 3348 (1996).
[4] A. Banerjee, S. Pal, and B. K. Chaudhuri, J. Chem. Phys. **115**, 1550 (2001).
[5] A. Banerjee, S. Pal, S. Bhattacharya, and B. K. Chaudhuri, J. Appl. Phys. **91**, 5125 (2002).
[6] R. Shreekala, M. Rajeswari, S. P. Pai, S. E. Lofland, V. Smolyaninova, K. Ghosh, S. B. Ogale, S. M. Bhagat, M. J. Downes, R. L. Greene, R. Ramesh, and T. Venkatesan, Appl. Phys. Lett. **74**, 2857 (1999).
[7] N. Khare, U. P. Moharil, A. K. Gupta, H. K. Singh, and O. N. Srivastava, J. Appl. Phys. **89**, 3532 (2001).

[8] Y. Matsumoto, J. Hombo, Y. Yamaguchi, M. Nishida, and A. Chiba, Appl. Phys. Lett. **56**, 1585 (1990).
[9] A. Oota, T. Horio, K. Ohba, and K. Iwasaki, J. Appl. Phys. **71**, 5997 (1992).
[10] D. Kumar, M. Sharon, P. R. Apte, R. Pinto, S. P. Pai, S. C. Purandare, C. P. D'Souza, L. C. Gupta, and R. Vijayaraghavan, J. Appl. Phys. **76**, 1349 (1994).
[11] L. I. Balcells, A. E. Carrillo, B. Martinez, and J. Fontcuberta, Appl. Phys. Lett. **74**, 4014 (1999).
[12] D. K. Petrov, L. Krusin-Elbaum, J. Z. Sun, C. Field, and P. R. Duncombe, Appl. Phys. Lett. **75**, 995 (1999).
[13] S. Gupta, R. Ranjit, C. Mitra, P. Raychaudhuri, and R. Pinto, Appl. Phys. Lett. **78**, 362 (2001).
[14] J. Gutierrez *et al.*, J. Phys.: Condens. Matter **12**, 10523 (2000); M. Uehara, S. Mori, C. H. Chen, and S. W. Cheong, Nature (London) **399**, 560 (1999).
[15] T. Tao, Q. Q. Cao, K. M. Gu, H. Y. Xu, S. Y. Xu, S. Y. Zhang, and Y. W. Du, Appl. Phys. Lett. **77**, 723 (2000).
[16] C. W. Sherle and S. T. Wang, Can. J. Phys. **48**, 2023 (1970).
[17] R. Mahendran, R. Mahesh, A. K. Raychaudhuri, and C. N. R. Rao, J. Phys. D **28**, 1743 (1995).
[18] X. Wen-Xu, L. Bao-He, Q. Zheng-Nan, and J. Han-Min, J. Appl. Phys. **86**, 5164 (1999).
[19] L. Pi, L. Zheng, and Y. Zhang, Phys. Rev. B **61**, 8917 (2000).
[20] N. Zhang, W. Ding, W. Zhong, D. Xing, and Y. Du, Phys. Rev. B **56**, 8138 (1997).
[21] N. F. Mott, J. Non-Cryst. Solids **1**, 1 (1968).
[22] M. Jaime, H. T. Hardner, M. B. Salamon, M. Rubinstein, P. Dorsy, and D. Emin, Phys. Rev. Lett. **78**, 951 (1997).
[23] A. Milner *et al.*, Phys. Rev. Lett. **76**, 475 (1996).
[24] J. L. Gittleman, Y. Goldstein, and S. Bozowski, Phys. Rev. B **5**, 3609 (1972).
[25] C. L. Chein, J. Appl. Phys. **69**, 5267 (1991); A. Marchand *et al.*, Science **28**, 2217 (1993).
[26] J. M. De Teresa *et al.*, Phys. Rev. B **54**, 1187 (1996).
[27] A. Urushibara *et al.*, Phys. Rev. B **51**, 14103 (1995).
[28] P. Schiffer, A. P. Ramirez, W. Bao, and S. W. Cheong, Phys. Rev. Lett. **75**, 3336 (1995).